# MAGNETIC CIRCUIT MODELING OF THE FIELD REGULATED RELUCTANCE MACHINE PART II: SATURATION MODELING AND RESULTS

Thomas J. Busch
Dept of Elect. Engr.
University of Idaho
Moscow, Idaho 83843

Joseph D. Law, Member, IEEE
Dept of Elect. Engr.
University of Idaho
Moscow, Idaho 83843

Thomas A. Lipo, Fellow, IEEE
Dept. of Elect. and Comp. Engr.
University of Wisconsin-Madison
Madison, Wisconsin 53706

*Abstract* – **This paper explores and offers solutions for two causes of simulation instabilities which occur when modeling machines using magnetic circuits. An algorithm for dynamic simulation of electric machines based on the magnetic circuit model (MCM) developed in Part I of this paper is augmented to include the ability to model magnetic saturation without numerical oscillations. The resulting MCM algorithm is implemented in a digital computer program which is well suited for both simulation of transients in non-sinusoidally wound machines such as a Field Regulated Reluctance Machine (FRRM), and for design. The model developed is verified using a laboratory prototype FRRM, converter, and controller. Results of computer simulations using the magnetic circuit model agree well with experimental machine data.**

**Keywords – Field Regulated Reluctance Machine, FRRM, Magnetic Circuit Modeling, MCM, Magnetic Saturation, Numerical Oscillations.**

## I. Introduction

In a prior work of the second author [1], numerical oscillations were observed to occur when modeling magnetic saturation. Historically, such numerical oscillations have limited the success of modeling electromagnetic devices using magnetic circuit models. In his most recent paper [2] on magnetic circuit modeling, Ostovic addresses the difficulty of instability in the solution of magnetic circuit model (MCM) equations. Ostovic's proposed solution to this problem results in the flux in each magnetic element being made a state variable which introduces additional complexity into the solution.

95 SM 476-2 EC A paper recommended and approved by by the IEEE Electric Machinery Committee of the IEEE Power Engineering Society for presentation at the 1995 IEEE/PES Summer Meeting, July 23-27, 1995, Portland, OR. Manuscript submitted January 3, 1995; made available for printing April 27, 1995.

It was observed in [3] that numerical oscillations in the MCM variables are the result of two causes. First, the solution for flux can oscillate if too large of a step size is used in the numerical solution of the MCM, even for linear magnetic characteristics. Second, the computed fluxes which are not linked by currents are susceptible to oscillation between parallel non-linear reluctances. In response to these problems, two solutions are proposed herein.

First, an implicit numerical integration method is employed to obtain a criterion for a step size that guarantees convergence for linear iron. A criterion for the implicit method reveals the dependence of a numerically convergent solution on the permeability of iron in magnetic saturation. A numerical analysis reference by Dahlquist [4] was utilized in the investigation of implicit numerical methods.

Second, a more comprehensive physical model that provides for damping is developed. In particular, it is shown that inclusion of the physical effect of eddy currents in the model prevents flux oscillations between parallel reluctances.

With the inclusion of saturation modeling, the resulting MCM algorithm is well suited for simulation of transients in non-sinusoidally wound machines such as a field regulated reluctance machine (FRRM), as well as for design. The model developed is verified using a laboratory prototype FRRM, converter, and controller. Results of computer simulations using the magnetic circuit model agree well with experimental machine data.

## II. Linear Implicit Convergence Criteria

In order to provide a robust integration algorithm, the A-stable implicit trapezoidal method has been chosen. The method [4] p. 347, is comprised of a first-order Euler predictor and a trapezoidal rule corrector, and can be readily adapted to solve the magnetic differential equations. A criterion exists [4] p. 347, which guarantees that corrector series of the trapezoidal rule predictor-corrector implicit method will converge for a first-order magnetic circuit. For a single-loop ferromagnetic structure of length $l$, uniform cross-sectional area, $A$, encircled by an $N$ turn excitation winding having resistance $r$, the follow differential equation holds,

$$\frac{d\lambda}{dt} = f(t,\lambda) = V - \frac{rl}{\mu A N^2}\lambda \tag{1}$$

The trapezoidal corrector series convergence criterion for Eqn. 1 follows.

$$\frac{1}{2}\Delta t \left\| \frac{\partial f(t,\lambda)}{\partial \lambda} \right\| = \frac{1}{2}\Delta t \left| -\frac{rl}{\mu A N^2} \right| < 1 \qquad (2)$$

Solving for $\Delta t$ in Eqn. 2 yields the maximum time step for which the corrector series of the implicit trapezoidal method will converge. It can be observed that the maximum allowable $\Delta t$ is dependent upon the minimum value of permeability, $\mu$. The permeability of magnetic material approaches a minimum value of $\mu_0 = 4\pi \times 10^{-7}$ in deep saturation.

Next, a two-loop ferromagnetic structure comprised of three parallel reluctances, $R_a$, $R_b$, and $R_c$, with uniform cross-sectional area, $A$, is investigated. An $N$ turn input winding having resistance $r$ encircles $R_a$. Such a structure represents the simplest case where flux paths in iron exist in parallel where one of the fluxes are not linking an external current. For the flux ($\lambda_1$) linking the winding current $I$:

$$\frac{d\lambda_1}{dt} = f(t,\lambda_1) = V - \frac{r\lambda_1}{N^2}\left(R_a + R_b - \frac{R_b^2}{(R_b + R_c)}\right) \qquad (3)$$

The trapezoidal corrector series convergence criterion for the two-loop structure is as follows.

$$\frac{1}{2}\Delta t \left| -\frac{r}{N^2}\left(R_a + R_b - \frac{R_b^2}{(R_b + R_c)}\right)\right| < 1 \qquad (4)$$

To find the maximum time step allowable for convergent modeling of deep magnetic saturation throughout the iron structure, Eqn. 4 is solved for $\Delta t$, using a minimum permeability value of $\mu_0$.

The time step in Eqn. 4 assures convergence of the trapezoidal corrector only for linear magnetization characteristics of minimum slope $\mu_0$. For nonlinear iron, the flux oscillates between $R_b$ and $R_c$ regardless of the size of the time step. The resulting oscillations in flux density between the parallel paths not linked by the input winding current are shown in Fig. 1.

Note that the flux density in $R_a$ is prevented from oscillating, even in deep saturation, by the input winding current limiting the time rate of change of flux in the iron. Flux also cannot change instantaneously in real electromagnetic materials due to the fact that eddy currents are induced to oppose a time rate of change in flux. A method of including eddy currents in simple magnetic circuit models is presented in the following section.

## III. Incorporating Effects of Physical Damping

A method for preventing the numerical oscillations in flux density between parallel paths appears to be realizable based on the behavior of flux in the two loop magnetic structure path which is encircled by a current. The current encircling this magnetic element limits the time rate of change of flux in the iron. As a result, the flux density

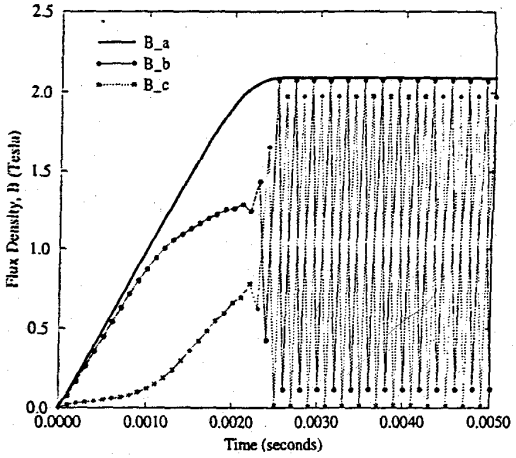


**Figure 1:** Two Loop Magnetic Structure Flux Densities for Nonlinear Magnetization Characteristics

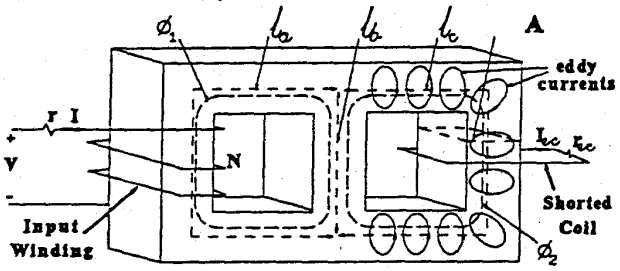


**Figure 2:** Two Loop Magnetic Structure with Eddy Current Coil

in this path is prevented from oscillating, even in deep saturation. Eddy currents constrain the time rate of change of flux in real electromagnetic materials, even if the flux is not linking an external current.

Figure 2 shows the two-loop magnetic structure studied previously, with a detailed cross-sectional view of the outer parallel path. This view shows the approximate location and orientation of the eddy currents induced encircling the flux flowing in $R_c$. In effect, there are an infinite number of single turn coils with infinitesimal electrical resistance distributed throughout the length of the iron path. Each of these coils can carry a different instantaneous current. A shorted coil of a single turn with a resistance, $r_{ec}$, representing the equivalent electrical resistance seen by the separate eddy currents will be used as an approximation.

For the two-loop ferromagnetic structure in Fig. 5, the following differential equations can be written

$$\frac{d\lambda_1}{dt} = f_1(\lambda_1,\lambda_2) = V - r\left(\frac{(R_a + R_b)}{N^2}\lambda_1 - \frac{R_b}{N^2}\lambda_2\right) \qquad (5)$$

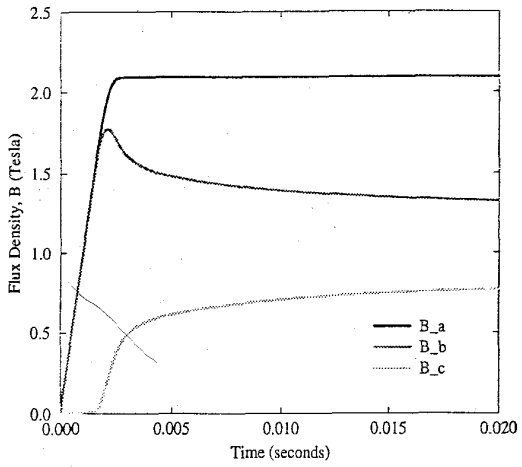


**Figure 3:** Flux Densities in a Two-Loop Magnetic Structure Including an Eddy Current Shorted Coil Model

$$\frac{d\lambda_2}{dt} = f_2(\lambda_1, \lambda_2) = r_{ec}\left(\frac{R_b}{N}\lambda_1 - (R_b + R_c)\lambda_2\right) \tag{6}$$

The implicit trapezoidal method can then be used to numerically solve the equations above. The convergence criterion can be found from the Euclidean norms of the following Jacobian array.

$$\begin{bmatrix} \frac{\partial f_1}{\partial \lambda_1} & \frac{\partial f_1}{\partial \lambda_2} \\ \frac{\partial f_2}{\partial \lambda_1} & \frac{\partial f_2}{\partial \lambda_2} \end{bmatrix} = \begin{bmatrix} \frac{r(R_a+R_b)}{N^2} & \frac{rR_b}{N} \\ \frac{r_{ec}R_b}{N} & -r_{ec}(R_b + R_c) \end{bmatrix} \tag{7}$$

To find the maximum time step for which the implicit method will convergently model saturation throughout the iron structure, a minimum of $\mu_0$ is substituted for the permeabilities of all the reluctances. The Euclidean norm of the second column is used to find the example $\Delta t$ given by the following expression.

$$\Delta t < \frac{2\mu_0 A}{\sqrt{(rl_b/N)^2 + r_{ec}^2(l_b + l_c)^2}} \tag{8}$$

Figure 2 plots the flux density levels $B_a$, $B_b$, and $B_c$, in the three parallel paths of the two loop structure shown in Fig. 5. For a simulation time step smaller than the criterion mandates, the implicit method converges to the correct flux density level in each of the three paths. The eddy current coil provides physically justifiable damping, preventing instantaneous changes in flux and eliminating numerical oscillations in flux density.

## IV. Eddy Currents in the FRRM MCM

Eddy currents circulating in the axial laminations of the FRRM rotor can be modeled as shorted electrical coils encircling iron elements. Non-magnetic interlamination layers provide unique flux loops in which to declare each eddy current path. Each coil constrains the eddy current it contains to have the same magnitude but opposite sign in the flux loops on either side of the lamination the coil encircles.

To simplify the development of the eddy current constraint equations, the following definitions are made. First, let $m$ equal the number of phases, and $n$ equal one less than the number of coils per phase belt. Set $p$ equal to the number of eddy current coils, and $l$ equal to the number of flux loops not linking either a phase or an eddy current. For the definitions above, the total number of stator phase currents per pole can be defined as $M = m + m \times n$. The total number of independent phase and eddy currents per pole, $P$, is equal to the number of phases plus the number of eddy current coils, or $P = m + p$. Finally, allow $Q$ to be the total number of constrained currents per pole face. As only $m$ phase currents and $p$ eddy currents are independent of each other, the remaining $Q = m \times n + p$ currents in $\mathbf{I}_{coil}$ are constrained. The loop flux matrix equation from Part I of this paper is restated here with a change of variables.

$$\begin{bmatrix} \mathbf{R}_{11} & \mathbf{R}_{12} \\ \mathbf{R}_{21} & \mathbf{R}_{22} \end{bmatrix} \begin{bmatrix} \mathbf{\Phi}_{coil} \\ \mathbf{\Phi}_{loop} \end{bmatrix} = \mathbf{N}^2 \begin{bmatrix} \mathbf{I}_{coil} \\ \mathbf{0} \end{bmatrix} \tag{9}$$

where $\mathbf{I}_{coil}$ is a vector of the coil currents, $\mathbf{\Phi}_{coil}$ is a vector of flux linking the coils, and $\mathbf{0}$ is a vector of zeros.

A new matrix, $\mathbf{N}$, is required to account for the differing number of turns between the stator windings of $N$ turns and the single turn eddy current coils, defined as follows:

$$\mathbf{N} = \begin{bmatrix} N\mathbf{U}_{m\times m} & \mathbf{0}_{m\times p} & \mathbf{0}_{m\times l} \\ \mathbf{0}_{p\times m} & \mathbf{U}_{p\times p} & \mathbf{0}_{p\times l} \\ \mathbf{0}_{l\times m} & \mathbf{0}_{l\times p} & \mathbf{U}_{l\times l} \end{bmatrix} \tag{10}$$

where $\mathbf{U}_{r\times r}$ is an $r \times r$ identity matrix and $\mathbf{0}_{r\times s}$ is an $r \times s$ matrix full of zeroes.

The current vector, $\mathbf{I}_{coil}$, has been augmented to include the eddy currents. The flux vector, $\mathbf{\Phi}_{coil}$, has been augmented to include the fluxes linking eddy currents.

$$[\ \mathbf{I}_{coil}\ ] = \begin{bmatrix} \mathbf{I}_{ph} \\ \mathbf{I}_{ec} \end{bmatrix} \text{ and } [\ \mathbf{\Phi}_{coil}\ ] = \begin{bmatrix} \mathbf{\Phi}_{ph\_b} \\ \mathbf{\Phi}_{ec} \end{bmatrix} \tag{11}$$

where $\mathbf{I}_{ph}$ is a vector of the phase currents, $\mathbf{I}_{ec}$ is a vector of the eddy currents, $\mathbf{\Phi}_{ph\_b}$ is a vector of the fluxes linking phase currents, and $\mathbf{\Phi}_{ec}$ is a vector of the fluxes linking eddy currents.

The set of scalar equations represented by the matrices in Eq. 9 are ordered such that the first $m$ elements of $\mathbf{I}_{coil}$ are each from a different stator phase. The next $p$ elements of $\mathbf{I}_{coil}$ are each from a different eddy current coil. The current vector $\mathbf{I}_{coil}$ is partitioned into two vectors, $\mathbf{I}_1$ and $\mathbf{I}_2$. The vector $\mathbf{I}_1$ contains the first $P = m+p$ elements of the vector $\mathbf{I}_{coil}$. Since there is only one coil per eddy current, the vector $\mathbf{I}_2$ contains elements $m+p+1 = P+1$ through $P+m\times n+p$ of the vector $\mathbf{I}_{coil}$.

The flux vector, $\Phi_{coil}$, is partitioned into two vectors, $\Phi_1$ and $\Phi_2$, in a similar manner. The reluctance matrices of Eq. 9 are partitioned such that the new reluctance matrices correspond to the partitioning of $\Phi_{coil}$.

The winding matrix defined in Part I of this paper can be augmented to incorporate the constraints governing the eddy currents. As a result $\mathbf{W}$ is now a $P \times Q$ winding matrix. Element $W_{kj}$ of the winding matrix $\mathbf{W}$ is defined by the two rules given in Part I of this paper in conjunction with the following requirement.

- Row $k$ of $\mathbf{W}$ contains a negative 1 in column $j$ ($W_{kj} = -1$) if the $j^{th}$ element of $\Phi_2$ links an eddy current flowing in the same shorted coil as the eddy current being linked by the $k^{th}$ element of $\Phi_1$.

By the above requirement, any given eddy current coil is constrained to have the same current in magnitude but opposite sign in adjacent flux loops when incorporated into the pre-multiplication of the reluctance matrix performed in Part I of this paper.

The time rate of change in the fluxes linking eddy currents, assuming a single resistance value, $r_{ec}$, for all the coils, is given by

$$0 = r_{ec}\mathbf{I}_{ec} + \frac{d\Phi_{ec}}{dt} \tag{12}$$

## V. Eddy Currents in MCM Torque Calculations

The energy converted from electrical to mechanical form is now given by:

$$\Delta W_{em} = \Delta W_{el} \pm \Delta W_{ec} - \Delta W_{fld} \tag{13}$$

where $\Delta W_{ec}$ is the energy generated or lost due to eddy currents, dependent upon whether the machine is acting as a motor or generator. The energy losses due to the eddy currents are given by

$$\Delta W_{ec} = \sum_{k=1}^{p} i_{ec_k}^2 r_{ec} \Delta t \tag{14}$$

## VI. Comparison of Computed and Tested Results

This section presents results from analyzing an experimental laboratory version of an FRRM with the Magnetic Circuit Model Program (MCMP). Figure 4 shows the primitive reluctance topology used to model the laboratory version FRRM. All pertinent machine specifications and dimensions for the FRRM modeled for this paper are presented in Table 1 of Appendix A.

Lengths and cross-sectional areas of the reluctances are equal to machine stator teeth, back iron, rotor iron and airgap dimensions, and are specific to the machine being modeled. Likewise, the reluctance permeabilities are dynamically established from the magnetization characteristics of the stator and rotor iron.

Figure 5 is a plot of the flux density levels in two parallel iron reluctances of the FRRM rotor model. The more

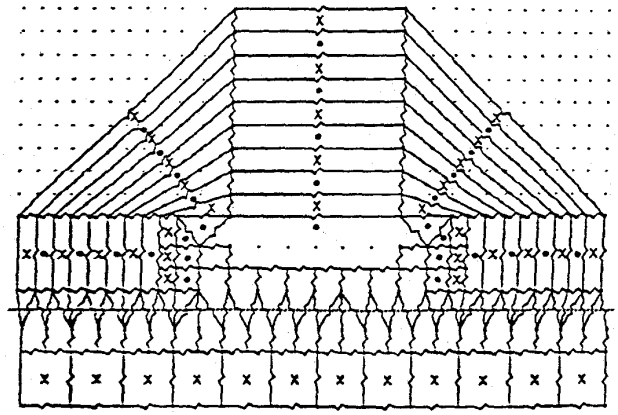

Figure 4: The primitive reluctance topology used to model the experimental FRRM is shown in this figure.

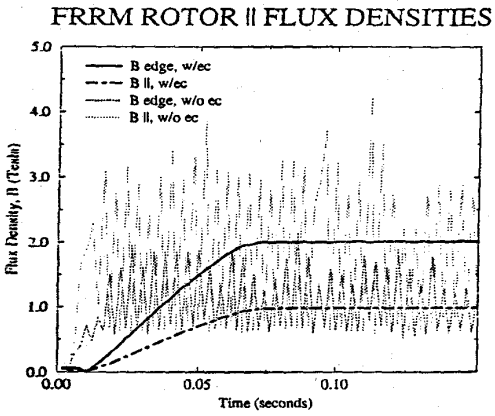


Figure 5: Flux Density Amplitude, B, in saturated parallel FRRM rotor pole face edge iron reluctances, with eddy currents modeled on the rotor and without.

saturated reluctance is located at the leading edge of a rotor pole face. Flux density oscillates between the parallel reluctances if eddy currents are not modeled on the rotor.

Figure 6 shows the close agreement between the self and mutual inductances for phase "a" of the laboratory FRRM obtained using the MCMP and experimental data.

The armature and field current references are maintained as equal to each other for all of the torque data presented. All of the torque, flux linkage, current, and voltages are given using a generator convention. Figure 7 shows the static torque versus rotor angle over 180 electrical degrees for 7.0 Amp phase currents. The large spikes are due to the rotor web midway across the pole face. The smaller torque variations are due to the pole edge interacting with the stator slots, i.e. slot harmonics. Note that the magnitude of the slot harmonics decrease about 90 electrical degrees. This decrease is partially due to the smoothing effect of the relatively long flux paths through

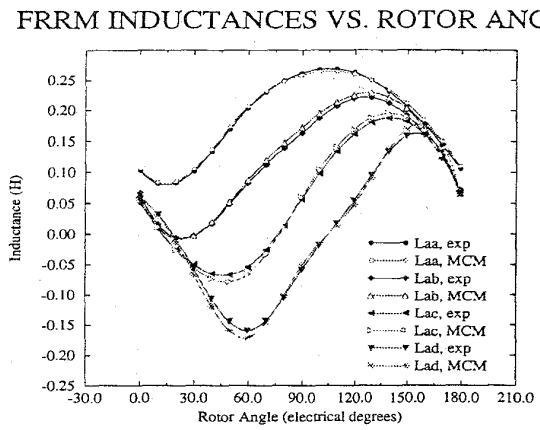


Figure 6: Self and mutual inductances for phase "a" of the laboratory FRRM obtained using the Magnetic Circuit Model Program compared to experimental data.

the interpole region. The decrease in the torque variation is also due to the fact that the rotor web is opposite stator teeth that have only a small amount of radial flux. Figure 8 shows the maximum average static torque over 30 electrical degrees as calculated by the MCMP and as obtained experimentally versus current magnitude. Armature reaction will clearly not have as large an effect if the flux density on the edge of the pole that has been weakened is still above the knee of the B versus H curve. This condition also exists in the laboratory FRRM.

For the machine under study, quasi-rectangular current excitation was regulated in the laboratory with a PWM Voltage Source Inverter. As a result, test current waveforms provide no significant information about the accuracy of the magnetic circuit machine model as a current regulator was also used in the simulations.

## VII. Summary

The magnetic circuit model of an FRRM based on loop equations developed in Part I of this paper is extended in this paper to include modeling of magnetic saturation. Equations describing the model provide the basis for simulation of an FRRM. A magnetic circuit model is developed for use in FRRM design, and a digital computer implementation of the magnetic circuit model is written. Test data used to verify the accuracy of the MCM was obtained from an FRRM machine, converter, and controller constructed in the laboratory.

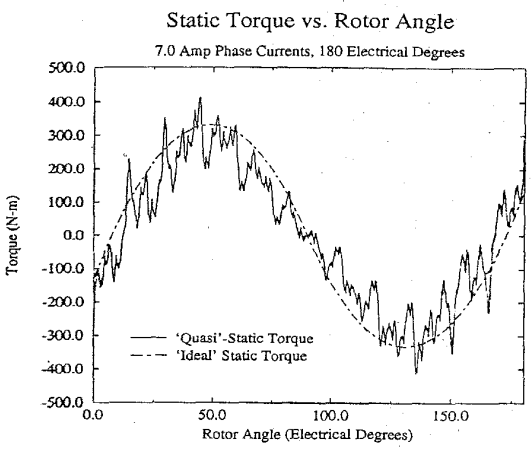


Figure 7: The static torque of the laboratory FRRM versus rotor angle is shown in this figure. The magnitude of the current command in both the field and armature phases is 7.0 amps. The data is obtained using the MCMP.

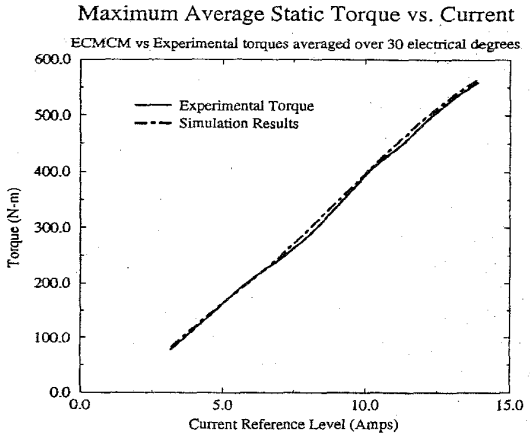


Figure 8: The maximum average static torque over 30 electrical degrees versus current is shown in this figure. The field and armature current commands are constrained to be equal. The data is obtained using the MCMP and from laboratory measurement.

Results of simulations performed using a software implementation of the magnetic circuit model are documented this article. Static torque and inductances calculated using the Magnetic Circuit Model Program, MCMP, agree closely with experimentally obtained results for the laboratory FRRM. The torque data clearly shows the effects of the stator slots and the rotor stainless steel web. That is, spatial effects are modeled by the MCMP.

The agreement of inductance and torque between the results of the MCMP and experimental results indicate that an MCM based on loop equations and modeling over only one pole is a valid approach. A MCMP based on loop equations can handle current and flux constraints in a simple manner. A simple algorithm can be used to implement the MCM.

## REFERENCES


[1] Law, J.D., *Modeling of Field Regulated Reluctance Machines*, Ph.D. Thesis, University of Wisconsin-Madison, 1991.

[2] Ostovic, V., "A Novel Method for Evaluation of Transient States in Saturated Electric Machines," *IEEE Trans. IAS*, Vol. 25, No. 1, Jan/Feb. 1989, pp. 96-100.

[3] Busch, T.J., *Modeling of Magnetic Saturation in Field Regulated Reluctance Machines*, M.S. Thesis, University of Idaho, 1994.

[4] Dahlquist, Germund, Björck, Åke, Anderson, Ned, *Numerical Methods*, Prentice-Hall Inc., 1974

[5] Law, J.D., A. Chertok, and T.A. Lipo, "Design and Performance of the Field Regulated Reluctance Machine," *IEEE Trans. IAS*, Vol. 30, No. 5, Sept./Oct. 1994, pp. 1185-1192.


## BIOGRAPHIES

See Part I.

## APPENDIX A

**Experimental Machine Specifications**

| | | |
|---|---|---|
| Power rating | 28.4 | kW |
| Force density | 19.2 | $kN/m^2$ |
| Power rating speed | 500 | RPM |
| Voltage per phase | 680 | Volts |
| Pole number | 6 | |
| Air-gap diameter | 27.3 | cm |
| Air-gap width | 0.0759 | cm |
| Axial length | 24.15 | cm |
| Radial distance pole center to air-gap | 2.09 | cm |
| Number of phases | 6 | |
| Number of field phases | 3 | |
| Number of armature phases | 3 | |
| Turns per phase per pole | 42 | |
| Amps @ rated power & speed | 13.9 | A |
| Current density,rms | 3.80 | $MA/m^2$ |
| Surface current density, rms | 47.0 | kA/m |
| Stator material | M43 | 21 mil steel |
| Rotor material | M6 | 14 mil steel |
| Air-gap magnetic flux density | 0.90 | tesla |

**Table A.1:** Laboratory FRRM Specifications